A Study of statistical description of interferometric SAR signal

S. REDADAA, A. BOUALLEG and M. BENSLAMA
ENST de Bretagne, Technopôle Brest-Iroise, CS 83818 –29238 Brest Cedex 3, France
Email : salah.redadaa@enst-bretagne.fr

Abstract: *Interferometric SAR data are frequently multi-look processed for speckle reduction and data compression. The statistical behavior of an interferometric signal is for great interest since it allows predicting its performance, and yet, few papers deal with the signal nature. This paper deals with the statistical behavior of the phase difference between two interferometric signals. The probability density function of interferometric signal is derived stating its dependence on the coherence and the mean of the phase difference. Besides, the Cramer-Rao lower bound (CRB) is also evaluated.*

Key words: *Synthetic aperture radar (SAR), interferometry, image, statistics.*

1. Introduction

The main feature of a SAR system, in front of conventional systems, is the azimuth resolution increase on the basis of carrying out a recording of complex data, as well as a coherent processing of such a data. Despite the SAR images complex nature, its phase does not carry information at all. On the other hand, SAR images are contaminated by speckle, a noise-like signal, although it is a true electromagnetic measurement [1]-[4].

The combination of different SAR images leads to multichannel SAR imagery. Any change in the sensor's geometry, in the operating frequency, in the employed polarization or the reflectivity scene will produce a change within the SAR image. In those cases, in which the changes gives rise to correlated images, the phase difference between the SAR images will contain useful information. When the SAR images are completely correlated, each of the individual images is contaminated by speckle, but the phase relation between them will contain useful information free of degrading factors.

There exist two main types of multichannel SAR imagery: SAR interferometry (InSAR) [5] and SAR polarimetry (PolSAR) [6]. The combination of these two data types, which called Polarimetric SAR Interferometry (PolInSAR) [7], is based on combining the advantages of each technique. This paper will be focused specially in InSAR.

SAR interferometry is basically based on the formation of an interferogram by using two complex SAR images of the same area, but acquired from slightly different positions. Therefore, the imagery geometry changes from the first SAR image to the second one. This change produces the phase difference between both SAR images to contain information about scene's topography. This system configuration is also called Across-Track interferometry [8]-[12], in contrast with Along-Track interferometry [13]-[15]. The two complex SAR images can be acquired either, simultaneously using two antennas in the same platform (single-pass interferometry) [16]-[17], or using the same system in repeated passes over the same scene (repeat-pass interferometry) [18]. In the later case, the phase difference between both SAR images will be also depend on possible scatterer variations between the different passes.

Due to the lack of knowledge about the detailed structure of the scatterer being imaged by the SAR system, it is necessary to discuss the properties of the scattered field statistically. The statistics of concern are defined over an ensemble of objects, all with the same macroscopic properties but differing in the internal structure. For a given SAR system imaging a particular scatterer, the exact value of each pixel can't be predicted, but only the parameters of the distribution describing the pixel values. Therefore, for a SAR image, the actual information per pixel is very low as individual pixels are simply random samples from distributions characterized by a set of parameters.

This paper is organized as follows. Section 2 introduces the geometric approach of SAR interferometry. In Section 3, we describe the statistical behavior of the phase difference. The probability density function of interferometric signal, in both single-look and multi-look cases, will

be derived stating its dependence on the absolute value of the correlation coefficient, and the mean of the phase difference. Besides, the Cramer-Rao lower band (CRB), is also derived. Finally, a conclusion is given.

2. SAR interferomerty

The interferometric SAR system is based on the geometry shown by Fig. 1. The use of this geometric approach makes possible to see the relationship between the surface and the sensor geometries in order to obtain the information contained within the SAR images difference. This approach is based on several simplifications as to consider a flat Earth or not considering signal spectral properties. Hence, the approximation is not valid for satellite geometries with large swaths or for airborne geometries. Detailed developments on SAR interferometry can be found in [3], [5], [8]-[9], [11]-[12].

Each of SAR platforms denoted by T_1 and T_2 respectively, acquires a SAR image. The two antennas are separated by a given baseline B, observing the same point P at range r from the first platform and at range $r+\Delta r$ from the second one. For the geometric approach, the observed point P will be assumed to be a point scatterer. Therefore, the two SAR images are

$$\begin{cases} s_1(x_1,r_1)=|s_1(x_1,r_1)|\exp(j\phi_1(x_1,r_1)) \\ s_2(x_2,r_2)=|s_2(x_2,r_2)|\exp(j\phi_2(x_2,r_2)) \end{cases} \quad (1)$$

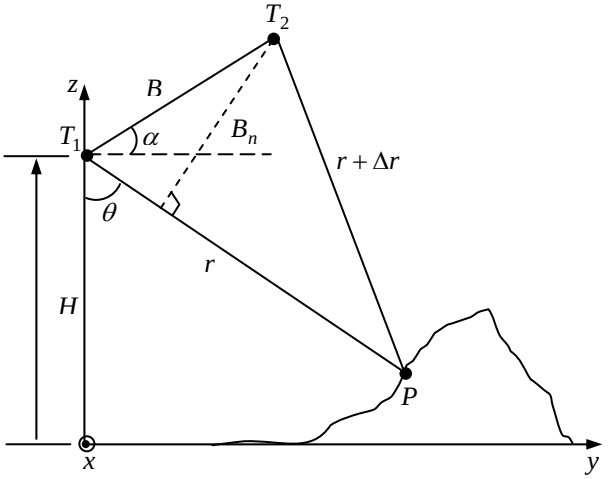

Fig. 1: Interferometric SAR system geometry.

Both SAR images observe the reflectivity scene from two different locations. Therefore, a given pixel of the first SAR image does not correspond to the same reflectivity contained in the pixel of the second image. There exist several techniques developed to solve this problem, known as image co-registering. In a classical approach, both images are registered, with a pixel accuracy, by using cross correlation techniques. In many cases, these techniques are not enough to obtain quality interferograms. To fulfil the quality requirements, sub-pixel registration techniques are employed [10], [19]. Once the SAR image pixels refer to the same area, the complex interferogram is defined as

$$s_1(x_1,r_1)s_2^*(x_2,r_2)=|s_1(x_1,r_1)||s_2(x_2,r_2)|\exp(j(\phi_1(x_1,r_1)-\phi_2(x_2,r_2))) \quad (2)$$

Owing to the fact that both SAR images observe the same point P from slightly different positions, the phase of each SAR can be written, taking into account the geometry depicted by Fig. 1, as

$$\begin{cases} \phi_1(x_1,r_1)=-\dfrac{4\pi}{\lambda}r+\phi_{s1} \\ \phi_2(x_2,r_2)=-\dfrac{4\pi}{\lambda}(r+\Delta r)+\phi_{s2} \end{cases} \quad (3)$$

Assuming that the phase due to the scatterer, ϕ_{s1} and ϕ_{s2}, are equal, the interferometric phase (i.e., the phase difference) is very sensitive measure for range difference

$$\Delta\phi = \phi_2 - \phi_1 = -\frac{4\pi}{\lambda}\Delta r + 2\pi k \tag{4}$$

Owing to the circular nature of any phase measurement, the interferometric phase given by (4) is ambiguous within integer multiples of 2π. In order to be able to relate the interferometric phase to the topographic height, the correct multiple 2π has to be added. This is done in the phase-unwrapping step after removing the flat-earth expected phase from the interferogram [20]-[21].

To derive the information content in $\Delta\phi$, it is necessary to see the dependence of Δr on the different parameters of the imaging geometry given by Fig. 1. Assuming this geometry, we have

$$(r+\Delta r)^2 = (r - B_r)^2 + B_n^2 \tag{5}$$

where

$$\begin{cases} B_n = B\cos(\theta-\alpha) \\ B_r = B\sin(\theta-\alpha) \end{cases} \tag{6}$$

wherein λ is the radar wavelength, θ is the look angle and α represents the tilt angle. B_r is called parallel baseline, whereas B_n is the perpendicular baseline. We suppose that the contribution of the term Δr^2 can be neglected in front of the parameter r. Therefore, Δr can be simplified as

$$\Delta r = \frac{B^2}{2r} - B\sin(\theta-\alpha) \tag{7}$$

The geometric approach for InSAR is based on a spaceborne system. In such a case, the difference between the baseline B and the range r is about several orders of magnitude, allowing to neglect the first addend in (7). Hence, Δr can be approximated by

$$\Delta r \approx -B\sin(\theta-\alpha) \tag{8}$$

With this approximation, the phase difference $\Delta\phi$, can be written as

$$\Delta\phi = \frac{4\pi}{\lambda}B\sin(\theta-\alpha) + 2\pi k \tag{9}$$

The equation (9) corresponds to the phase of a single pixel in the interferogram. However, this phase is not useful as the wavelength is so short that the phase is wrapped, apart from the fact that is also contains range information.

From (9), the interferometric phase error can be expressed as

$$\delta\Delta\varphi = \frac{4\pi B}{\lambda}\cos(\theta-\alpha)\delta\theta \tag{10}$$

Since the elevation error is evaluated as [3], [5]

$$\frac{\Delta z}{z} = \tan(\theta)\delta\theta = \frac{\lambda\tan(\theta)}{4\pi B\cos(\theta-\alpha)}\delta\Delta\varphi \tag{11}$$

3. Probability density of interferometric phase

In this section, we introduce the probability density function (pdf) of the phase difference in both single-look and multi-look cases. First a data model is presented defining the statistical types of variables cartographic radars deal with. This data model is based upon a zero-mean Gaussian hypothesis .The signal emitted by a radar illuminate a given area, commonly called resolution cell, which is limited by the pulse length and the look angle. The received signal is reflected by elementary particles of the resolution cell, called scatterers. In this paper, we study the interferometric signal depending on statistical behavior of these scatterers. This analysis is carried out in both single-look and multi-look cases.

3.1 Single-look

The information received by the two interferometric sensors can be modeled [22]-[23] by

$$\begin{cases} s_1 = x_1 + jy_1 = r_1 \exp(j\phi_1) \\ s_2 = x_2 + jy_2 = r_2 \exp(j\phi_2) \end{cases} \tag{12}$$

where x_i and y_i are zero-mean Gaussian distributed, r_i has a Rayleigh distribution of parameter σ_r^2, and ϕ_i is a uniform random variable distributed on the interval $[-\pi, \pi[$. As the sum of independent, identically distributed sacatters are complex Gaussian distributed by the Central Limit Theorem, the probability density function of bivariate complex Gaussian vector s is [24]

$$P_S(s) = \frac{1}{\pi^2 |K|} \exp\left\{ s^{*T} K^{-1} s \right\} \tag{13}$$

where $s = [s_1 \quad s_2]^T$ is the data vector which is an outcome of the random variable S, K is the covariance matrix of s, $|.|$ is the determinant of $(.)$, and $(.)^T$ and $(.)^{*T}$ represent the transpose and the conjugate transpose of $(.)$, respectively. Considering that the real and imaginary parts of s_i are uncorrelated, let us define the following notation

$$\begin{aligned} &E\{s_i\} = 0 \\ &E\{x_i^2\} = E(y_i^2) = \sigma_i^2/2 \\ &E(x_1 y_1) = E(x_2 y_2) = 0 \\ &E(x_1 x_2) = E(y_1 y_2) = \sigma/2 \\ &E(x_1 y_2) = -E(y_1 x_2) = \eta/2 \end{aligned} \tag{14}$$

where $E\{.\}$ stands for the expected value of $(.)$. Thus, the signal s is a second-order circular process since, by definition, for all $\phi \in \Re$, the moments of s defined by $s_i = r_i \exp(j\phi_i)$ up to second order are identical to the corresponding moments of r [25]. Note that since σ and η are not null, s_i is partially decorrelated.

Let us introduce now the correlation coefficient that will be needed to evaluate the covariance matrix K. The complex correlation coefficient statically measures the degree of relationship between two sensors. It is, thus, defined by the expected value of the inter-sensor cross product as follows

$$\gamma = \frac{E\{s_1 s_2^*\}}{\sqrt{E\{s_1 s_1^*\}}\sqrt{E\{s_2 s_2^*\}}} \equiv |\gamma| \exp(j\psi) \tag{15}$$

where $|\gamma|$ is the coherence, and ψ is the phase of the complex correlation coefficient. Note that the correlation coefficient can be written from (14) as follows

$$\gamma = \frac{\sigma - j\eta}{\sigma_1 \sigma_2} \tag{16}$$

Likewise, the covariance matrix has the form

$$K = E\{ss^*\} = \begin{pmatrix} \sigma_1^2 & \sigma_1 \sigma_2 \gamma \\ \sigma_1 \sigma_2 \gamma^* & \sigma_2^2 \end{pmatrix} \tag{17}$$

then, the single-look phase difference is obtained by interfering both sensors as

$$\Delta\phi = \arg(s_1 s_2^*) \tag{18}$$

In the following, the single-look phase distribution is derived. To do so, we consider the definitions given by (14). The inverse of the covariance matrix K defined by (17) is

$$K^{-1} = \frac{1}{D^2} \begin{pmatrix} \sigma_2^2 & -\sigma_1 \sigma_2 \gamma \\ -\sigma_1 \sigma_2 \gamma^* & \sigma_1^2 \end{pmatrix} \tag{19}$$

where $D^2 = \sigma_1^2 \sigma_2^2 \left(1 - |\gamma|^2\right)$. The distribution can be written as

$$P_S(s_1, s_2) = \frac{1}{(\pi D)^2} \exp\left\{ -\frac{1}{D^2} \left(\sigma_2^2 r_1^2 + \sigma_1^2 r_2^2 - 2\sigma_1 \sigma_2 \operatorname{Re}\{\gamma^* s_1 s_2^*\} \right) \right\} \tag{20}$$

Changing the rotational coordinates by means of the transformation

$$\begin{pmatrix} r_1 \\ \psi_1 \\ r_2 \\ \psi_2 \end{pmatrix} \rightarrow \begin{pmatrix} s_1 = r_1 \exp(j\phi_1) \\ s_2 = r_2 \exp(j\phi_2) \end{pmatrix} \tag{21}$$

Its Jacobian matrix determinant is $r_1 r_2$, and supposing that $\sigma_1 = \sigma_2 = \sigma$, the joint pdf becomes

$$P(r_1, r_2, \phi_1, \phi_2) = \frac{r_1 r_2}{(\pi D)^2} \exp\left\{ -\frac{r_1^2 + r_2^2 - 2 r_1 r_2 |\gamma| \cos(\Delta\phi - \psi)}{\sigma^2 \left(1 - |\gamma|^2\right)} \right\} \tag{22}$$

In order to derive the single-look phase distribution, the following changes of variable are used

$$\begin{pmatrix} z \\ v \end{pmatrix} \rightarrow \begin{pmatrix} r_1 = \frac{1}{\sqrt{2}} \sqrt{\sigma^2 \left(1 - |\gamma|^2\right)} z^{1/2} \exp(v/2) \\ r_2 = \frac{1}{\sqrt{2}} \sqrt{\sigma^2 \left(1 - |\gamma|^2\right)} z^{1/2} \exp(-v/2) \end{pmatrix} \tag{23}$$

Whose Jacobian matrix determinant is

$$|\det(J)| = \frac{\sigma^2 \left(1 - |\gamma|^2\right)}{4} \tag{24}$$

So (22) becomes

$$\begin{aligned} P(z, v, \varphi_1, \varphi_2) &= \frac{1 - |\gamma|^2}{2(2\pi)^2} z \exp\left\{ -\frac{1}{2} \left[z \exp(v) + z \exp(-v) - 2z\beta \right] \right\} \\ &= \frac{1 - |\gamma|^2}{2(2\pi)^2} z \exp\{ -z \cosh(v) \} \exp\{ 2z\beta \} \end{aligned} \tag{25}$$

where

$$\beta = |\gamma| \cos(\Delta\phi - \psi) \tag{26}$$

Integrating with respect to z and v,

$$P(\phi_1, \phi_2) = \frac{1 - |\gamma|^2}{(2\pi)^2} \int_0^{+\infty} z \exp(\beta z) K_0(z) dz \tag{27}$$

where $K_0(z)$ is a modified Bessel function of the second kind. Then (27) gives

$$P(\phi_1, \phi_2) = \frac{1 - |\gamma|^2}{(2\pi)^2} \left[\frac{1}{1 - \beta^2} + \frac{\beta}{\left(1 - \beta^2\right)^{3/2}} \left(\frac{\pi}{2} + \sin^{-1}(\beta) \right) \right] \tag{28}$$

which depends on $\Delta\phi$. In order to evaluate the phase distribution, we have

$$P(\Delta\phi) = \int_0^{2\pi} P(\Delta\phi, \phi) d\phi \tag{29}$$

So, finally the single-look phase distribution is

$$P(\Delta\phi) = \frac{1 - |\gamma|^2}{2\pi} \left[\frac{1}{1 - \beta^2} + \frac{\beta}{\left(1 - \beta^2\right)^{3/2}} \left(\frac{\pi}{2} + \sin^{-1}(\beta) \right) \right] \tag{30}$$

Fig.2 depicts the single-look phase difference distribution for $|\gamma| = 0, 0.4, 0.7,$ and $0.90,$ $\psi = 0$. It shows that for high coherence values, the mean-centered distribution gets sharper and narrower resembling to a delta function, while for low coherence values, the phase distribution tends to a uniform distribution.

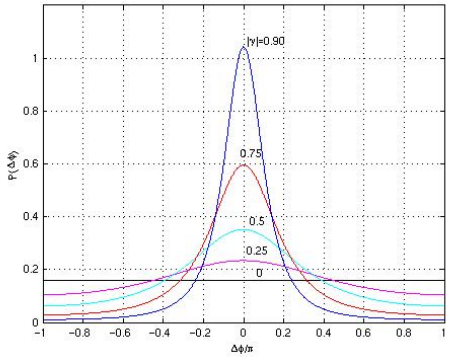

Fig. 2 Interferometric phase pdf for different coherence values.

On the other hand, the theoretical single-look variance of a fluctuating signal was derived by Tough et al. [23] and takes the form

$$\mathrm{var}(\Delta\phi) = \frac{1-|\gamma|^2}{1-|\gamma|^2\cos^2(\psi)}\left\{\frac{\pi^2}{4} - \pi\sin^{-1}(|\gamma|\cos\psi) + \left[\sin^{-1}(|\gamma|\cos\psi)\right]^2\right\} + \frac{1}{2}\sum_{i=1}^{\infty}\frac{1-|\gamma|^{2i}}{i^2} \tag{31}$$

Fig. 3 shows the numerically computed standard deviation of $\Delta\phi$ vs. coherence for $\psi = 0$.

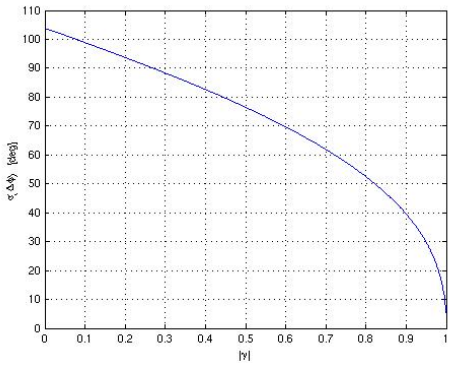

Fig. 3 Interferometric phase standard deviation.

3.2 Multi-look analysis

Multi-look techniques arise as a way to decrease the noise level of a single look process. N consecutive samples of the interferometric signal envelope are taken to average the final value. This low-pass filter technique is regarded as a likelihood estimator [23] which corresponds to the peak of the correlation function.

Let us generally define s as a (Nxq) complex data matrix with a $\aleph(0, K)$ distribution. Thus, the multi-look likelihood estimator is obtained by

$$z_{ij} = \frac{1}{N}s_i s_j^* = \frac{1}{N}\sum_{n=1}^{N} s_i^{(n)} s_j^{(n)*} \tag{32}$$

Since $s^{(1)}, s^{(2)}, \ldots, s^{(N)}$ are independent, identically complex $\aleph(0, K)$ distributed, $W = NZ$ has a Wishart probability distribution of covariance matrix K, and N degrees of freedom [26]. Its complex probability density function (pdf) is given by

$$P_W(\omega) = \frac{|\omega|^{N-q-1}}{\Gamma_q(N/2)|K|^N}\exp\left\{-Tr\left(K^{-1}\omega\right)\right\} \tag{33}$$

where $Tr(.)$ denotes the trace of $(.)$, K is defined by (17), q is the dimension of $s^{(i)}$, and $\Gamma_q(N/2)$ is the multivariate gamma function defined as [27]

$$\Gamma_q(N/2) = \pi^{q(q-1)/2}\prod_{j=1}^{q}\Gamma(N+1-j) \tag{34}$$

Regarding the interferometric case $(q = 2)$, and expressing ω as

$$\omega = \begin{pmatrix} \omega_{11} & \omega_{12} \\ \omega_{21} & \omega_{22} \end{pmatrix} \tag{35}$$

then, the multi-look phase difference $\Delta\phi$ is the argument of ω_{12}

$$\omega_{12} \equiv \alpha\exp(j\Delta\phi) = \omega_{21}^* \tag{36}$$

where α is defined as the absolute value of ω_{12}. Considering the above equations, the distribution of Z is given as

$$P_Z(z)=\frac{N^{qn}|z|^{N-q-1}}{\Gamma_q(N/2)|K|^N}\exp\{-Tr(K^{-1}z)\} \tag{37}$$

To determine, the multi-look phase distribution, the expression (35) is inserted into (33) obtaining

$$P(\omega,\alpha,\Delta\phi)=\frac{(\omega_{11}\omega_{22}-\alpha^2)^{N-2}}{\pi\Gamma(N)\Gamma(N-1)\sigma_1^{2N}\sigma_2^{2N}(1-|\gamma|^2)^N}.\exp\left\{-\frac{1}{D^2}\left[\sigma_2^2\omega_{11}+\sigma_1^2\omega_{22}-2\sigma_1\sigma_2|\gamma|\alpha\cos(\Delta\phi-\psi)\right]\right\} \tag{38}$$

Using the following changes of variable

$$u_1=\frac{\omega_{11}}{\sigma_1^2}\quad u_2=\frac{\omega_{22}}{\sigma_2^2}\quad v=\frac{\alpha}{\sigma_1\sigma_2} \tag{39}$$

We get

$$P(u_1,u_2,\eta,\Delta\phi)=\frac{(u_1u_2-v^2)^{N-2}v}{\pi\Gamma(N)\Gamma(N-1)(1-|\gamma|^2)^N}.\exp\left\{-\frac{1}{1-|\gamma|^2}\left[u_1+u_2-2v|\gamma|\cos(\Delta\varphi-\psi)\right]\right\} \tag{40}$$

The multi-look phase distribution is derived by integrating (40) over u_1,u_2 and v and is evaluated as [28]-[31]

$$P(\Delta\phi)=\frac{\Gamma(N+1/2)}{\Gamma(N)}\frac{(1-|\gamma|^2)^N}{2\sqrt{\pi}}\frac{\beta}{(1-\beta^2)^{2N+1/2}}+\frac{(1-|\gamma|^2)^N}{2\pi}{}_2F_1(N,1;1/2,\beta^2) \tag{41}$$

where ${}_2F_1(N,1;1/2,\beta^2)$ is a Gauss hypergeometric function [32], and β is defined by (26). In [2] and [23], another expression, involving a finite summation based upon the characteristic function of Fourier transform domain, is derived. In this case, the marginal pdf is

$$P(\Delta\phi)=\frac{(1-|\gamma|^2)^N}{2\pi}\left\{\begin{array}{l}\frac{(2N-2)!}{[(N-1)!]^2\,2^{2(N-1)}}\cdot\left[\frac{(2N-1)\beta}{(1-\beta^2)^{N+1/2}}\cos^{-1}(-\beta)+\frac{1}{(1-\beta^2)^N}\right]+\frac{1}{2(N-1)}\\ \cdot\sum_{r=0}^{N-2}\frac{\Gamma(N-1/2)}{\Gamma(N-1/2-r)}\frac{\Gamma(N-1-r)}{\Gamma(N-1)}\frac{1+(2r+1)\beta^2}{(1-\beta^2)^{r+2}}\end{array}\right\} \tag{42}$$

The phase distribution, (40), involves the hypergeometric function, which must be calculated by numerical quadrature. By contrast, (41) involves only a finite summation that is more convenient for data analysis. Note that when $N=1$, the summation contains no terms and the distribution reduces to the single-look case (29). Fig.4 shows the phase difference distribution tends to a Dirac delta function as the number of looks increases.

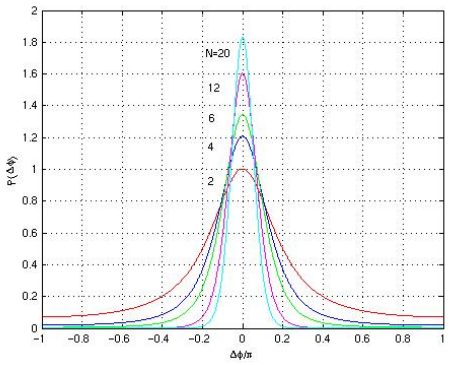

Fig. 4 Interferometric phase pdf for different number of look for $(|\gamma|=0.8,\psi=0)$.

3.3 Cramer Rao lower bound

Here, we evaluate the Cramer-Rao lower bound (CRB) of the phase difference estimation using the signal data model introduced previously, i.e., for a zero-mean complex Gaussian circular signal s.

The variance characterizes the second-order statistical behaviorof an estimator, and is often used to know its efficiency. Indeed, an unbiased estimator $\hat{\theta}$ is efficient from a statistical point of view when its variance reaches the minimum value. This asymptotical minimum value id defined by the CRB [33, 34] as

$$\mathrm{var}\left\{\hat{\theta}\right\} \geq I^{-1}(\theta) \tag{43}$$

where $I(\theta)$ is the Fisher information matrix given by

$$I(\theta) = -E\left\{\frac{\partial^2 \ln P(s;\theta)}{\partial \theta^2}\right\} \tag{44}$$

where $P(s;\theta)$ is the joint distribution function of s and θ.

In this paper, we derive the CRB of phase difference estimator for a single-look distribution. The log-likelihood function of (13) is

$$\ln P_S(s_1, s_2) = const - \frac{1}{D^2}\exp\left\{-\frac{1}{D^2}\left(\sigma_2^2 r_1^2 + \sigma_1^2 r_2^2 - 2\sigma_1\sigma_2\ \mathrm{Re}\left\{\gamma^* s_1 s_2^*\right\}\right)\right\} \tag{45}$$

where $\gamma \equiv |\gamma|\exp(j\omega\tau)$, $D^2 = \sigma_1^2\sigma_2^2\left(1-|\gamma|^2\right)$ and $\mathrm{Re}\{.\}$ stands for the real part of $\{.\}$. Note that only γ depends on the integration variable τ. In addition, we suppose that we are close to the peak of correlation. Thus, $|\gamma|$ does note change during the evaluation of the CRB. So, the expected value of (45) is

$$E\left\{\frac{\partial^2 \ln P_S(s_1, s_2)}{\partial \tau^2}\right\} = \frac{2\sigma_1\sigma_2}{D^2} E\left\{\mathrm{Re}\left\{\frac{\partial^2 \gamma^*}{\partial \tau^2} s_1 s_2^*\right\}\right\} \tag{46}$$

Next, by evaluating the second derivation of γ^* and since by definition

$$E\left\{s_1 s_2^*\right\} = |\gamma|\sigma_1\sigma_2\exp(j\omega\tau) \tag{47}$$

we have

$$E\left\{\frac{\partial^2 \ln P_S(s_1, s_2)}{\partial \tau^2}\right\} = \frac{2}{1-|\gamma|^2}\mathrm{Re}\left\{-|\gamma|\omega^2 e^{-j\omega\tau}|\gamma|e^{j\omega\tau}\right\} = -2\omega^2\frac{|\gamma|^2}{1-|\gamma|^2} \tag{48}$$

Finally, using the following relation between the SNR and the coherence [18]

$$|\gamma| = \frac{1}{1+SNR^{-1}} \tag{49}$$

The CRB of the time delay is

$$\mathrm{var}(\tau) \geq \frac{1}{\omega^2 SNR}\left(1+\frac{1}{2SNR}\right) \tag{50}$$

Since $\Delta\phi = \omega\tau$, the CRB of the phase difference is

$$\mathrm{var}(\Delta\phi) \geq \frac{1}{SNR}\left(1+\frac{1}{2SNR}\right) \tag{51}$$

Now, we derive the CRB of phase difference estimator for a multi-look distribution. The same assumptions for the single-look case are considered here. This minimum variance bound is obtained as follows

$$\mathrm{var}(\tau) \geq -\left(E\left\{\frac{\partial^2 \ln P_Z(z;\tau)}{\partial \tau^2}\right\}\right)^{-1} \tag{52}$$

First, we determine the log-likelihood function of (37)

$$\ln P_Z(z) = const - NTr\left(K^{-1}z\right) \tag{53}$$

where K^{-1} is defined by (19). Evaluating the trace of the product, we get

$$\ln P_Z(z) = const - \frac{N}{D^2}\left(\sigma_2^2 z_{11} + \sigma_1^2 z_{22} - 2\sigma_1\sigma_2 \operatorname{Re}\left\{\gamma^* z_{12}\right\}\right) \tag{54}$$

Note that when deriving (54), only γ depends on the integration variable τ. In addition, we suppose that we are close to the peak of correlation. Thus, $|\gamma|$ does note change during the evaluation of the CRB. So, the expected value of (54) is

$$E\left\{\frac{\partial^2 \ln P_Z(z)}{\partial \tau^2}\right\} = \frac{2N\sigma_1\sigma_2}{D^2} E\left\{\operatorname{Re}\left\{\frac{\partial^2 \gamma^*}{\partial \tau^2} z_{12}\right\}\right\} \tag{55}$$

The expected value of (55) only affects to z_{12} since γ is not random variable. In order to determine its value, we suppose that the backscatterer signal process is ergodic. Thus, the coherence coefficient does not depend on the observation time. The expected value of z_{12} is

$$E(z_{12}) = E\left\{\frac{1}{N}\sum_{k=1}^{N} s_1^{(k)} s_2^{*(k)}\right\} = \frac{1}{N}\sum_{k=1}^{N} E\left\{s_1^{(k)} s_2^{*(k)}\right\} = \frac{1}{N}\sum_{k=1}^{N} \sigma_1\sigma_2\gamma = |\gamma|\sigma_1\sigma_2 \exp(j\omega\tau) \tag{56}$$

Evaluating the second derivation of γ^*, and inserting (56) into (55), we get

$$E\left\{\frac{\partial^2 \ln P_Z(z)}{\partial \tau^2}\right\} = \frac{2N}{1-|\gamma|^2} \operatorname{Re}\left\{-|\gamma|\omega^2 e^{-j\omega\tau}|\gamma| e^{j\omega\tau}\right\} = -2N\omega^2 \frac{|\gamma|^2}{1-|\gamma|^2} \tag{57}$$

Finally, inserting (49) into (57), the CRB of the time delay is

$$\operatorname{var}(\tau) \geq \frac{1}{\omega^2 N.SNR}\left(1 + \frac{1}{2SNR}\right) \tag{58}$$

Since $\Delta\phi = \omega\tau$, the CRB of the phase difference is

$$\operatorname{var}(\Delta\phi) \geq \frac{1}{N.SNR}\left(1 + \frac{1}{2SNR}\right) \tag{59}$$

Conclusion

In this paper, after a general presentation of SAR interferometry, the mutual relationships between the interferometric phase and the different parameters of the imaging geometry are presented.

The probability density function of interferometric signal, in both single-look and multi-look cases, is derived and discussed for a data model which is based upon a zero-mean Gaussian hypothesis. We have also evaluated the Cramer-Rao lower bound of the phase difference estimation using the same signal data model.

References

1. J. C. Curlander, R. N. McDonough, Synthetic Aperture Radar: Systems and Signal Processing. New York: John Wiley & Sons, 1991.
2. C. Olivier, S. Quegan. Understanding Synthetic Aperture Radar Images. Artech House, Inc., 1998.
3. G. Franceshetti, R. Lanari. Synthetic Aperture Radar Processing. CRC Press LLC., 1999.
4. H. Maître. Traitement des Images de Radar à Synthèse d'Ouverture. Hermes Science, 2001.
5. D. Massonnet , T. Rabaute. Radar interferometry: Limits and potential. IEEE Trans. Geosci. Remote Sensing , vol. 31, no.2, pp. 455-464, 1993.
6. F. T. Ulaby, C. Elachi. Radar Polarimetry for Geoscience Applications. Artech House, Norwood MA, 1990.
7. S. R Cloude, K. P. Papathanassiou. Polarimetric SAR interferometry. IEEE Trans. Geosci. Remote Sensing, vol. 36, no5, pp.1551-1165, 1998.
8. L. C. Graham. Synthetic aperture radar interferometer for topographic mapping. Proc. IEEE, vol. 62, pp. 763-768, 1974.
9. Z. A. Zebker, R. M. Goldstein. Topographic mapping from interferometric synthetic aperture radar observations. J Geophysical Research, vol. 91, pp. 4993-499, 1986.
10. A. K. Gabriel, R. M. Goldstein. Crossed orbit interferometry: theory and experimental results from SIR-B. Int J Remote Sensing, vol. 9, no.5, pp. 857-872, 1988.
11. E. Rodriguez, J. Martin. Theory and design of interferometric synthetic aperture radars. IEE Proc.-F, vol. 139, pp. 147-159, 1992.
12. P. A. Rosen, F. K. Li, S. Hensley et al. Synthetic aperture radar interferometry. Proc. IEEE, vol. 88, pp. 333-382, 2000.
13. R. M. Goldstein, T. P. Barnett, H. A. Zebker. Remote sensing of oceans currents. Science, vol. 246, pp. 1282-1285, 1989.
14. L. P. Orwig, D. N. Held. Interferometric ocean surface mapping and moving object relocation with a norden systems Ku-band SAR. IEEE Int Geosci. Remote Sensing Symposium, pp. 1598-1600, 1992.
15. E. Chapin, C. W. Chen. Preliminary results from an airborne experiment using along-track interferometry for ground moving target indication," IEEE International Radar Conference, pp. 343-347, 2005.
16. R. Scheiber. Along- and across-track single-pass interferometry using the E-SAR system," IEEE Int Geosci. Remote Sensing Symposium, pp. 1097 –1099, 1998.
17. J. J. Mallorqui, I. Rosado, M. Bara. Interferometric calibration for DEM enhancing and system characterization in single pass SAR interferometry. IEEE Int Geosci. Remote Sensing Symposium, pp. 404-406, 2001.
18. R. Lanari, G. Fornaro, D. Riccio et al. Generation of digital elevation models by using SIR-C/X-SAR multifrequency two-pass interferometry: the Etna case study. IEEE Trans. Geosci. Remote Sensing, vol. 34, no.5, pp. 1097-1114, 1996.
19. H. A. Zebker, C. L. Werner, P. A. Rosen, S. Hensley. Accuracy of topographic maps derived from ERS-1 interferometric radar. IEEE Trans. Geosci. Remote Sensing , vol. 32, no.4, pp. 823-836, 1994.
20. D. C. Ghiglia, L. A. Romero. Robust two-dimensional weighted and unweighted phase unwrapping that uses fast transforms and interactive methods. J Optical. Society of America A, vol. 11, pp.107-117, 1994.
21. R. M Goldstein, H. A. Zebker, C. L. Werner. Satellite radar interferometry: Two-dimensional phase unwrapping. Radio Science, vol. 23,: pp.713-720, 1988.
22. R. J. A. Tough, D. Blacknell, S. Quegan. Estimators and distributions in single and multi-look polarimetric and interferometric data. IEEE Int Geosci. Remote Sensing Symposium, pp. 2176-2178, 1994.

23. R. J. A. Tough, D. Blacknell, S. Quegan. A statistical description of polarimetric and interferometric synthetic aperture radar data, Proceedings of the Royal Society , vol. 449, pp. 567-589, 1995.
24. A. Papoulis. Probability, Random Variables, and Stochastic Processes. McGraw Hill editions, 1991.
25. T. Chonavel. Statistical Signal Processing, Modelling and Estimation. Springer, 2002.
26. J. Wishart. The generalized product moment distribution in samples from a normal multivariate population. Biometrika , pp. 32-52, 1928.
27. N. R. Goodman. Statistical analysis based on a certain multivariate complex Gaussian distribution (an introduction). Annals Math. Stat., vol. 34, pp. 152-177, 1963.
28. J. S. Lee, A. R. Miller, K. W. Hoppel. Statistics of phase difference and product magnitude of multilook complex Gaussian signals. Waves in Random Media, vol. 4, pp. 307-319, 1994.
29. I. R. Joughin, D. P. Winebrenner, D. B. Percival. Probability density functions for multilook polarimetric signatures. IEEE Trans. Geosci. Remote Sensing , vol. 32, no. 3, pp. 562-574, 1994.
30. B. C. Barber. The phase statistics of multichannel radar interferometer. Waves in Random Media, vol. 3, pp. 257-266, 1993.
31. J. S. Lee, K. W. Hoppel, S. A. Mango, A. R. Miller. Intensity and phase statistics of multilook polarimetric and interferometric SAR imagery. IEEE Trans. Geosci. Remote Sensing, vol. 32, no.5, pp. 1017-1028, 1994.
32. M. Abramowitz, I. A. Stegun. Handbook of Mathematical Munctions, New York: Dover Publications Inc, 1972.
33. H. V. Poor. An Introduction to Signal Detection and Estimation. Springer-Verlag, 1998.
34. S. M. Kay. Fundamentals of Statistical Signal Processing, Estimation Theory, Prentice Hall International, Inc., 1993.

Article received: 2006-12-28